RESEARCH ARTICLE

INTERNATIONAL JOURNAL OF
ENERGY RESEARCH | WILEY

Alkali metal modified iron-nickel oxygen carrier to produce hydrogen-rich synthesis gas by chemical looping gasification with pine sawdust

Pengcheng Wang[1,2] | Ge Pu[1,2] (iD) | Qiwen Liu[1,2] | Weicheng Xiong[1,2]

[1]Key Laboratory of Low-Grade Energy Utilization Technologies and Systems, Ministry of Education, Chongqing University, Chongqing, China

[2]School of Energy and Power Engineering, Chongqing University, Chongqing, China

Correspondence
Ge Pu, Key Laboratory of Low-Grade Energy Utilization Technologies and Systems, Ministry of Education, School of Energy and Power Engineering, Chongqing University, Chongqing 400044, China.
Email: puge@cqu.edu.cn

Summary

In the research of biomass chemical looping gasification technology, the production of hydrogen-rich synthesis gas has received increasing attention. In this paper, iron-nickel oxygen carriers were prepared by the mechanical and impregnation method. Chemical looping gasification experiments were performed with pine sawdust in a self-built fixed-bed reactor to prepare hydrogen-rich synthesis gas. Experimental results showed that for the iron-nickel oxygen carrier with a loading ratio of 3% NiO under reaction conditions of 800°C, ratio of steam content to biomass (S/B) of 1.25, and ratio of lattice oxygen to biomass (O/B) of 0.2, the volume fraction of hydrogen in the synthesized gas reached 43.06%; correspondingly, the carbon conversion rate was 78.22%, the low calorific value of syngas was 7.49 MJ/Nm^3, and the gas production rate was 1.25 Nm^3/kg. After modification of the iron-nickel oxygen carrier with a mass ratio of 5% K$_2$CO$_3$, the volume fraction of hydrogen in the prepared synthesis gas increased to 47.83%, the corresponding carbon conversion rate was 85.44%, and the low-level calorific value was 7.95 MJ/Nm^3. The gas production rate was 1.49 Nm^3/kg.

KEYWORDS

alkali metal, chemical looping gasification, Fe-Ni oxygen carrier, hydrogen-rich synthesis gas, pine sawdust
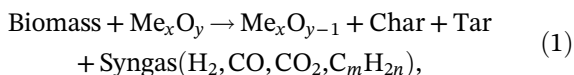
1 | INTRODUCTION

Biomass energy is a low-carbon energy source, which is abundant reserves, environmentally friendly, and renewable.[1-4] Biomass pyrolysis gasification technology converts biomass energy into high-quality fuel gas. At present, the traditional gasification methods have the disadvantages of low energy efficiency, high gas production cost, and complex systems.[5,6] In order to improve gas quality and reduce production costs, biomass chemical looping gasification technology is proposed.[7] Biomass chemical looping is an emerging gasification technology.[8] Lattice oxygen in an oxygen carrier is used to provide oxygen for the gasification of biomass.[9] By controlling the ratio of lattice oxygen to biomass fuel, after biomass gasification to obtain H$_2$, synthesis gas is produced, consisting mainly of CO.[10-13] Chemical looping gasification technology has many advantages, such as the following: The oxygen carrier provides lattice oxygen in the CLG process, which does not need to consume oxygen and can be reused. So it reduces the reaction cost. The main component of hydrogen-rich syngas produced by gasification reaction is H$_2$ and CO. And the CLG process reduces the tar output and exergic loss, and improves the calorific value of syngas.[14-16]

The CLG system is composed of an air reaction and a fuel reactor, as shown in Figure 1. The fuel is introduced

to the fuel reactor, which contains a metal oxide (Me_xO_y) that is called oxygen carrier. The outlet gas from the fuel reactor contains CO, H_2, CO_2, and C_nH_m. After biomass undergoes a chemical looping gasification reaction, the carbon that is not fully reacted will form tar. Then, the reduced metal oxide (Me_xO_{y-1}) is transferred to the air reactor where the oxygen carrier is oxidized. The main reactions are shown as equations of (1) and (2):

$$\text{Biomass} + Me_xO_y \rightarrow Me_xO_{y-1} + \text{Char} + \text{Tar} + \text{Syngas}(H_2, CO, CO_2, C_mH_{2n}), \tag{1}$$

$$Me_xO_{y-1} + O_2 \rightarrow Me_xO_y, \tag{2}$$

The oxygen carrier is the key component of chemical looping gasification technology. At present, oxygen carriers that have been studied at home and abroad include transition metal oxides, such as Fe, Cu, Ni, and Mn, as well as low-cost oxygen carriers such as $CaSO_4$ and natural ore.[17-21] However, there are many deficiencies in single metal oxygen carriers, so a research trend is to add modified substances to a single metal oxygen carrier.[22,23] Among them, Fe-based oxygen carriers have the advantages of low cost, wide sources, environmental friendliness, strong sintering resistance, and so on, but their biggest disadvantage is their relatively low reactivity.[24-26] Therefore, the introduction of modified substances in iron-based oxygen carriers, to improve their reactivity, has great research potential.[27]
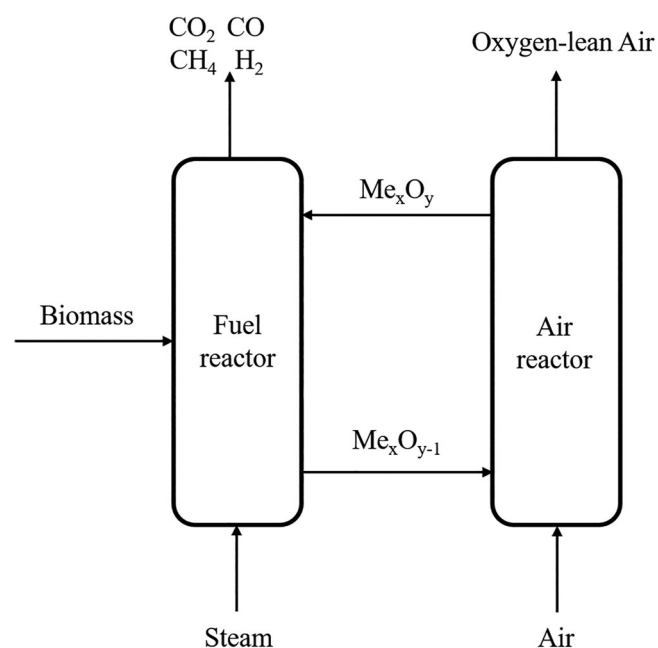

FIGURE 1 Schematic presentation of chemical looping process

Huang et al[28] used NiO to modify hematite, which significantly improved the reactivity and reaction performance of the oxygen carrier. Huang et al[29] prepared $NiFe_2O_4$ and reacted it with biomass char on a fixed bed. The results showed that the activity of $NiFe_2O_4$ was significantly higher than that of Fe_2O_3 alone and mechanically mixed $Fe_2O_3 + NiO$. This is due to the synergy of Fe/Ni in the unique spinel structure. Chen et al[30] prepared four iron-based MFe_2O_4 (M = Cu, Ba, Ni, and Co) composite oxygen carriers by the sol-gel method, and carried out chemical looping gasification reaction with coke, pyrolysis gas, and toluene in order to prepare hydrogen-rich synthesis gas. Studies have shown that all four ferrites are attractive for chemical gasification processes, and because of their metal synergy in the crystal structure, they have good oxygen transfer properties and a wide distribution of metal cations. Feng et al,[31] through density functional theory (DFT) calculations, simulated and evaluated 18 potential dopants of iron-based oxygen carriers. The results showed that the doping of alkali metal K by iron-based oxygen carriers enhanced the reduction reaction of Fe_2O_3 to Fe_3O_4, and also improved the Fe_3O_4 to FeO. Huang et al[32] prepared $NiFe_2O_4$ oxygen carrier to investigate chemical looping steam reforming to produce hydrogen, and introduced inert alumina. As a result, $NiFe_2O_4$ sintering was effectively suppressed, and the reactivity and recoverability of oxygen carrier particles were significantly improved.

Based on Fe-based oxygen carriers, we loaded NiO in different proportions and performed gasification reaction with pine sawdust on a fixed bed to find the optimal NiO load ratio, the best steam content biomass ratio, and the reaction temperature. Then, it was modified with alkali metal K_2CO_3 to find the optimal load ratio of K_2CO_3, further improve the activity of oxygen carriers, and prepare hydrogen-rich synthesis gas.

2 | EXPERIMENTAL MATERIALS AND DEVICES

2.1 | Biomass raw materials

In this experiment, the biomass used was common pine sawdust. The sample was dried in a drying box at 105°C for 6 hours, and then 30 to 60 mesh pine sawdust particles were sieved out by a sieve and loaded into a sample bag. The air was released from the sample bag, and it was placed in a dry dish for later use.

The results of elemental analysis of sieved and dried pine sawdust using an elemental analyzer are shown in Table 1.

Among the above elements, C and H can reduce the oxygen carrier and promote the release of lattice oxygen. The mass concentrations of C, H, and O in the pine wood are 48.78%, 6.49%, and 44.35%, respectively. They are the main reaction substances in the fuel reactor. The content of N and S is relatively small, and the content of NO_X and SO_X produced by the reaction in the synthesis gas is less than 0.1%, which has negligible influence on the reaction calculation; so N and S can be ignored in actual calculations.

2.2 | Oxygen carrier preparation

The raw materials used for the production of oxygen carrier included Fe_2O_3 powder, $Ni(NO_3)_2 \cdot 6H_2O$ crystal, and K_2CO_3 powder. The raw materials were provided by Chengdu Cologne Chemical Co., Ltd., with analytical reagent (AR) grade purity and content of raw materials of 99.0%.

The Fe/Ni composite oxygen carrier was prepared by analyzing the pure Fe_2O_3 powder and $Ni(NO_3)_2 \cdot 6H_2O$ crystals as raw materials by the mechanical and impregnation method. A certain mass of Fe_2O_3 powder was weighed, pressed into a tablet at a pressure of 30 MPa using a tablet press, and then calcined in a muffle furnace at 850°C for 6 hours in an air atmosphere. After taking it out, it was ground and 40 to 150 mesh particles were screened out with a sieve, taken in a sample bag, and the bag was sealed. According to different mass ratios of Fe/Ni, a certain mass of $Ni(NO_3)_2 \cdot 6H_2O$ crystals was weighed and put into a beaker, and an appropriate amount of water was added to dissolve. Then, in a water bath at a constant temperature of 60°C, Fe_2O_3 particles were impregnated in a $Ni(NO_3)_2 \cdot 6H_2O$ solution at a constant temperature for 24 hours. After full immersion, the particles were put into a drying oven and dried for 12 hours at 80°C. Finally, the dried material was put into a muffle furnace and calcined in an air atmosphere at 850°C for 6 hours. After calcining, it was taken out and ground. Then, a sample sieve was used to sieve out 40 to 150 mesh particles, which were put into a sample bag to obtain the desired target oxygen carrier.

In the preparation of Fe/Ni/K composite oxygen carrier, according to the mass ratio of K_2CO_3, a certain mass of analytically pure Fe_2O_3 powder and K_2CO_3 powder were weighed and fully mixed in a mixing dish. Then, a tablet press was used to form tablets. The remaining steps were the same as those described above.

2.3 | Material characterization

The crystal phase and cell size of the samples were provided by high-efficiency conventional powder x-ray diffractometer (XRD; PANalytical X′ Pert Powder). The specific surface area and pore volume of the specified samples were analyzed by a surface area and pore size analyzer (BET, Quadrasorb 2MP). The surface morphology and characteristics of the samples were determined by scanning electron microscopy (SEM) on an FEI Tecnai G2 F20 instrument. A field emission transmission electron microscope was used to observe and analyze the high-resolution surface morphology of the oxygen carrier at 200 KV.

2.4 | Experimental equipment and process

The experimental system comprises a small fixed-bed reaction system, consisting of a gas distribution system, a fixed-bed reaction system, and a gas analysis system. The fixed-bed reaction system uses a vertical heating furnace, with a maximum furnace temperature of 1000°C and error less than 10°C. After the reactor is put into the vertical furnace heater, the furnace door is closed, and the upper and lower ends are sealed with insulating cotton to prevent large heat loss, resulting in the actual temperature in the constant temperature zone being lower than the temperature shown on the panel. The gasification reactor uses a quartz tube reactor with an inner diameter of 26 mm, wall thickness of 3 mm, and length of 900 mm, and a partition plate is arranged 400 mm from the end so that reaction materials can be loaded in the tube to carry out the reaction. The injection pump uses a one-way pump provided by Baoding Shenchen Pump Industry Co., Ltd. The gas chromatograph used for gas composition detection is the Agilent 7890B. This gas chromatograph can accurately detect the concentration of CO_2, CO, H_2, CH_4, C_mH_n, N_2, and other gases with high accuracy. It is the most reliable gas detection equipment at present.

The inert carrier gas used in the experiment was N_2 with a flow rate of 60 mL/min. Steam enters the reactor through an injection pump, vaporizes it at high temperature in the furnace, and enters the reaction zone together with the carrier gas. After the reaction, the gas is dried and collected by a gas collection bag. Finally, the gas chromatograph used for gas composition detection is the Agilent 7890B (Agilent Technologies, USA) with an

TABLE 1 Elemental analysis of pine samples (%, air-dried basis)

Ultimate analysis				
C	H	O	N	S
48.78	6.49	44.35	0.01	0.37

Agilent column (DB-WAXETR, length: 30 m, inner diameter: 0.53 mm, film thickness: 1 μm). A schematic diagram of the system is shown in Figure 2.

2.5 | Experimental method and data analysis

2.5.1 | Experimental method

Chemical looping gasification of biomass was carried out in a fixed-bed reactor. The temperature was regulated by the temperature controller on the vertical heating furnace, the reaction temperature was set, and then the programmed temperature rise was started. In the reaction process, the injection pump injects deionized water into the fixed-bed reactor through a steel needle with a diameter of 0.2 mm, uses the high temperature in the heating furnace to gasify the water, and brings it into the reaction area under the purging of inert N_2 carrier gas to participate in the reaction. The specific steps of the chemical looping gasification experiment are as follows:

1. Checking the air tightness of the whole gas circuit. The reaction system was purged by N_2 with a flow rate of 1 L/min before experiments started.
2. The reactor was heated up to 800°C by the furnace at a heating rate of 10°C/min under N_2 atmosphere, according to the predetermined program.
3. When the temperature reaches the design value, the constant flow pump is used to inject different volumes of deionized water into the reactor. Then, send the mixture of oxygen carrier and pine sawdust into the reactor through the feed port.
4. Connect the gas collecting bag to the end of the gas pipeline, start timing, close the valve of the gas collecting bag and the injection pump after 50 minutes, purge the reactor with N_2 for 20 minutes, then change the gas path to O_2, and enter O_2 to oxidize the oxygen carrier after reaction for 50 minutes, which completes the cycle.

2.5.2 | Data analysis

The data analysis method of this experiment is described as follows:

The peroxide coefficient α is the ratio of the mass of oxygen provided by the oxygen carrier added to the reaction system to the mass of oxygen required for complete oxidation of biomass.[29] The calculation formula is as follows:

$$\alpha = \frac{m_{O_2}}{m_l}, \qquad (3)$$

where m_{O_2} and m_1 represent the mass of oxygen released by the added oxygen carrier in the reaction system and the mass of oxygen required for the complete oxidation of pine sawdust, respectively.

The ratio of steam content to biomass (S/B) is defined as the ratio of the mass of steam content flowing into the reactor to the mass of biomass.[29] The calculation formula is as follows:
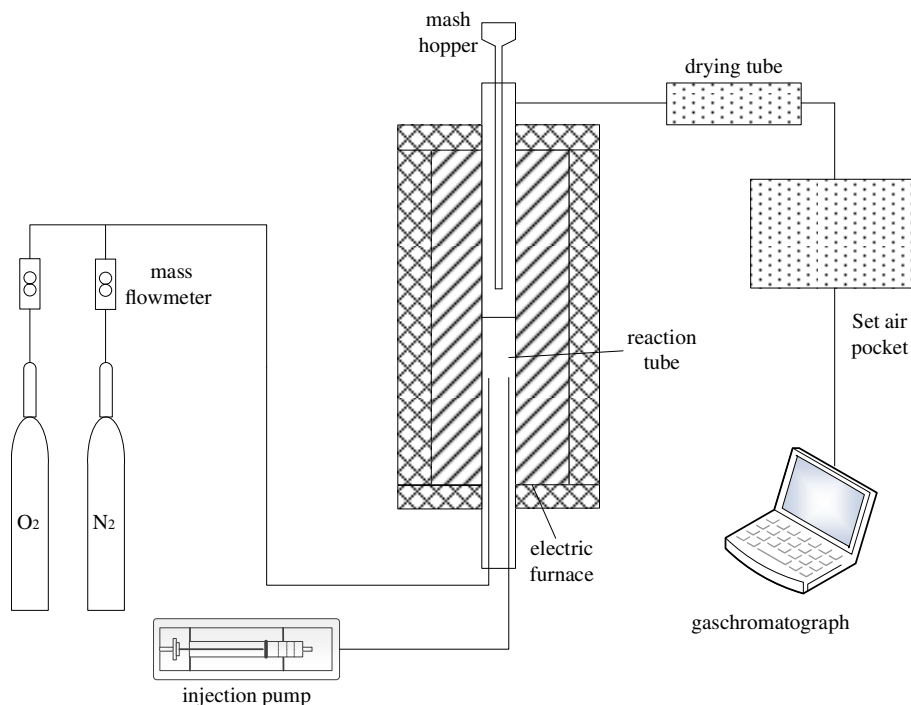

FIGURE 2 Schematic diagram of the fixed-bed reaction system [Colour figure can be viewed at wileyonlinelibrary.com]

$$S/B = \frac{mS}{mB}, \qquad (4)$$

where m_S and m_B represent the mass of steam content and biomass added to the reactor, respectively.

The volume concentration C_i (Nm^3) of each component in the syngas is calculated using the following formula[17]:

$$Ci = \frac{Vi}{(V_{H_2} + V_{CO_2} + V_{CO} + V_{CH_4})} \times 100\%, \qquad (5)$$

where V_i represents the volume of a certain gas (H_2, CO_2, CO, CH_4).

The syngas yield, G_V (Nm^3/kg), is defined as the volume of gas produced by biomass per unit mass under standard conditions.[29] The calculation formula is as follows:

$$G_V = \frac{V_{H_2} + V_{CO_2} + V_{CO} + V_{CH_4}}{m_{bio}}, \qquad (6)$$

where V_{H2}, V_{CO2}, V_{CO}, and V_{CH4} represent the volume of H_2, CO_2, CO, and CH_4, respectively, and m_{bio} represents the mass of biomass used in each group of experiments.

The carbon conversion rate, η_c, is an important parameter to evaluate biomass gasification.[29] It is defined as the ratio of the carbon content of the gas produced in the reduction stage to the carbon added into the reactor. The calculation formula is as follows:

$$\eta_c = \frac{12 \times (C_{CO_2} + C_{CO} + C_{CH_4}) \times G_V}{22.4 \times (298/273) \times C\%} \times 100\%, \qquad (7)$$

where G_V is gas yield; C_{CO2}, C_{CO}, and C_{CH4} represent the volume percentage of CO_2, CO, and CH_4 in syngas, respectively; and $C\%$ represents the carbon fraction in the biomass.

The lower calorific value of syngas, LHV (MJ/Nm^3), is calculated by the following formula[17]:

$$LHV = 0.126C_{CO} + 0.108C_{H_2} + 0.359C_{CH_4}, \qquad (8)$$

where C_{H2}, C_{CO}, and C_{CH4} represent the volume percentage of H_2, CO, and CH_4 in syngas, respectively.

3 | RESULTS AND DISCUSSION

3.1 | Fe/Ni research

3.1.1 | Iron-nickel phase characterization

An iron-nickel composite oxygen carrier with a nickel loading mass ratio of 3% was taken and subjected to XRD characterization after calcining. The result was shown in Figure 3.

As shown in Figure 3, iron-nickel composite oxide peaks appeared at $2\theta = 30.2°$, $35.4°$, $43.2°$, and $62.5°$, which coincided with the characteristic peaks of $NiFe_2O_4$,[29] so, after calcining, there was a spinel between iron and nickel stone structure of $NiFe_2O_4$ composite oxide. The XRD characterization results show that the main substances of the iron-based oxygen carrier doped with NiO are Fe_2O_3 and $NiFe_2O_4$. Due to the low doping amount of NiO, Fe_2O_3 is still the main component in the oxygen carrier, and Fe_2O_3 is the main oxygen releasing substance in the CLG process.

3.1.2 | Effect of loading different proportions of NiO

Under the conditions of reaction temperature of 800°C, peroxide coefficient of 0.2, and steam/biomass ratio of 1.0, the optimal loading ratio of NiO was investigated. The carrier gas was N_2, the flow rate was 60 mL/min, and the reaction time was 50 minutes. The experimental results are shown in Figure 4.

As shown in Figure 4, with increased NiO load, the volume concentration of H_2 in the synthesis gas increased from 37.18% to 41.36%, and then began to decrease. The volume concentration of CO kept rising, increasing from 15.58% to 18.10%. The volume concentration of CO_2 decreased from 44.02% to 39.91%, and then began rising. The volume concentration of CH_4 in the synthesis gas slowly decreased.

In addition, as the load of NiO increased, the carbon conversion rate increased from 61.78% to 75.82%, but the
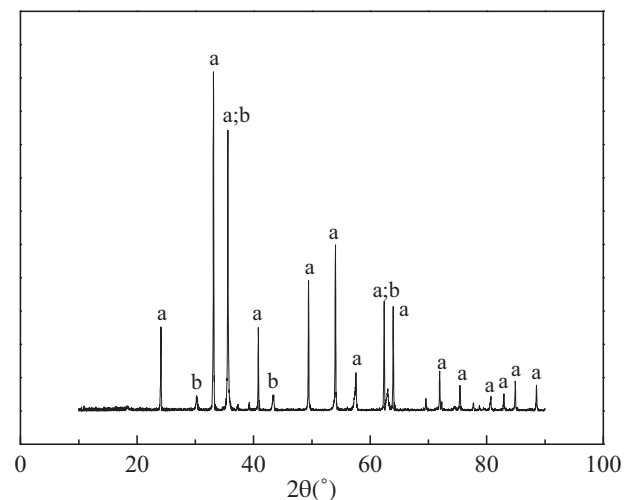

FIGURE 3 XRD pattern of a sample with a nickel loading mass ratio of 3%: A, Fe_2O_3; B, $NiFe_2O_4$

slope of the curve is the largest at the 3% load, which means that the carbon conversion rate achieved maximum growth rate. At a load of 3%, the low calorific value of syngas achieved a maximum of 7.28 MJ/Nm^3, and the corresponding yield was 1.15 Nm^3/kg.

The loaded NiO can form a unique NiFe$_2$O$_4$ spinel structure with Fe$_2$O$_3$. This spinel structure has a strong oxygen release ability, which can make the oxygen carrier reach a deeper degree of reduction in a shorter reaction time, so NiFe$_2$O$_4$ compared to Fe$_2$O$_3$ is more suitable for CLG process. However, the loaded NiO will lose oxygen along with Fe$_2$O$_3$ during the reaction process. NiO has apparent selectivity to H$_2$ (H$_2$ + NiO → Ni + H$_2$O). Excessive loading of NiO will consume H$_2$ in the synthesis gas and reduce the H$_2$ content, thus resulting in the calorific value of syngas reduced.[33]

In summary, the proper loading of NiO on the iron-based oxygen carrier has a significant effect on promoting the chemical gasification reaction of the biomass. Under this operating condition, when the loading mass ratio of NiO was 3%, the proportion of H$_2$ reached the maximum, and the calorific value of syngas at the low level was also the largest.

3.1.3 | Effect of steam content/biomass ratio

The presence of steam content as a gasification agent in the gasification reaction plays a vital role in obtaining high-quality syngas.[33] The effects of different steam content/biomass ratios were explored at a reaction temperature of 800°C and a peroxide factor of 0.2. The experimental results are shown in Figure 5.

In the process of biomass chemical looping gasification reaction, introducing the appropriate amount of steam content can promote the gasification reaction of solid fuel; at the same time, it can apparently improve the yield of hydrogen and the quality of synthesis gas. As shown in Figure 5, with S/B increasing from 0.5 to 1.25, the volume concentration of H$_2$ in the syngas continued to rise, from 36.09% to 43.06%; the volume concentration of CO decreased from 19.10% to 16.42%; and the volume concentration of CO$_2$ decreased from 42.80% to 38.40%. At S/B = 1.25, the carbon conversion rate and low calorific value of synthesis gas reach the maximum values of 78.22% and 7.49 MJ/Nm^3, respectively. As the amount of steam content continued to increase, the carbon conversion rate and low calorific value of synthesis gas began to decrease. This is because excessive steam content will consume heat in the furnace, causing changes in the temperature.
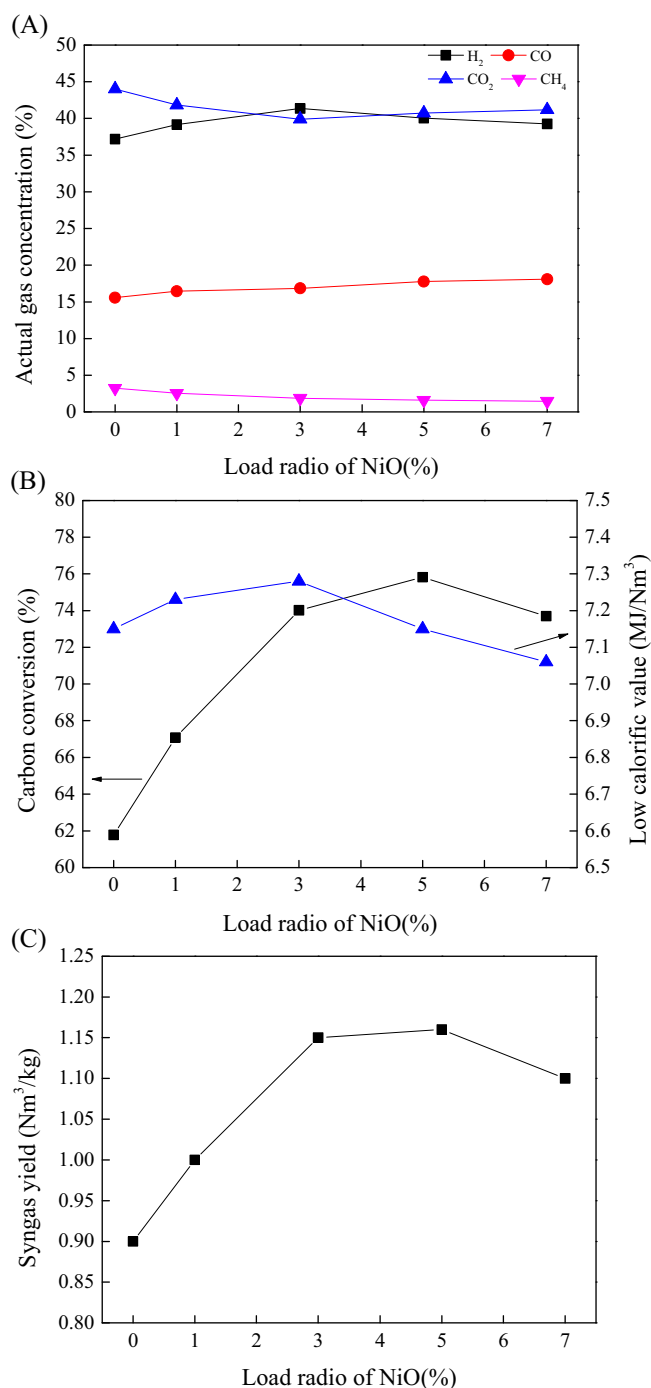

FIGURE 4 Effect of loading different proportions of NiO: A, syngas composition; B, carbon conversion rate and low calorific value; C, syngas yield. Reaction conditions: T = 800°C, ratio of lattice oxygen to biomass (O/B) = 0.2, ratio of steam content to biomass (S/B) = 1.0, N$_2$ flow rate of 60 mL/min, reaction time of 50 minutes [Colour figure can be viewed at wileyonlinelibrary.com]

In summary, appropriately increasing S/B has an obvious promotion effect on the gasification reaction of biomass chemical looping. At S/B = 1.25, the volume concentration of H$_2$ in syngas was 43.06%, the carbon
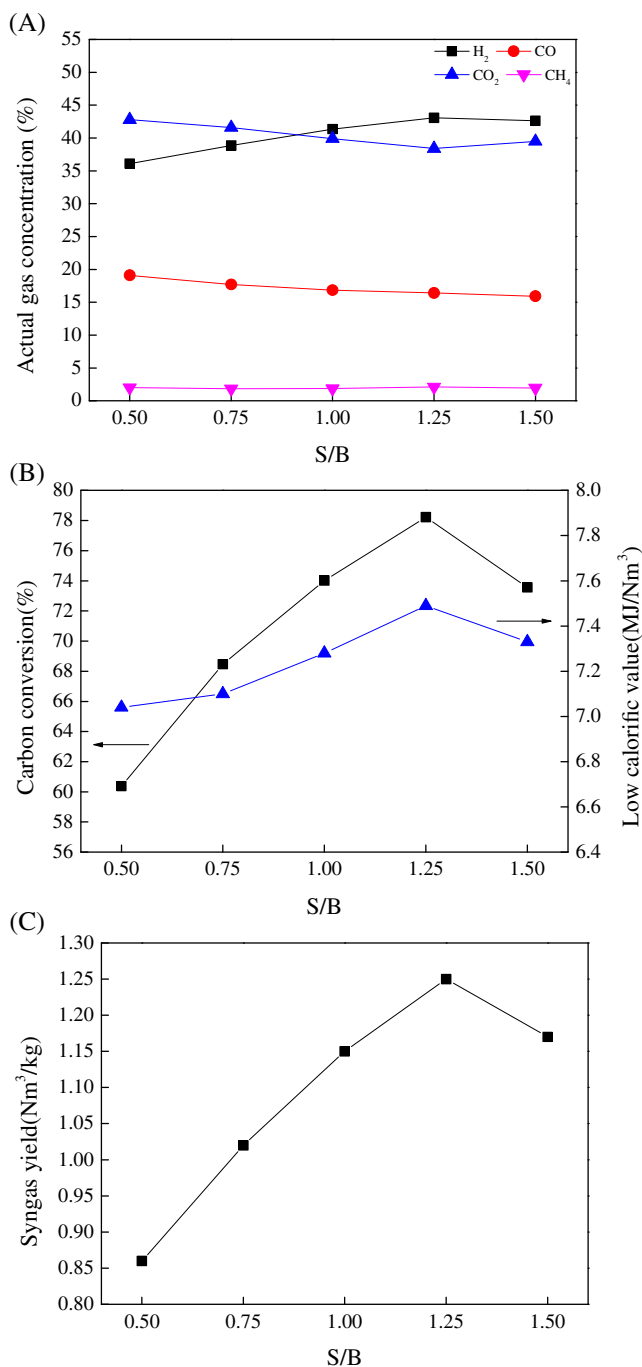
(A)

(B)

(C)

FIGURE 5 Effect of steam content/biomass ratio: A, syngas composition; B, carbon conversion rate and low calorific value; C, syngas yield. Reaction conditions: T = 800°C, O/B = 0.2, N$_2$ flow rate of 60 mL/min, reaction time of 50 minutes [Colour figure can be viewed at wileyonlinelibrary.com]

conversion rate was 78.22%, the low calorific value was 7.49 MJ/Nm^3, and the yield was 1.25 Nm^3/kg.

Appropriate increase of steam can promote the conversion of fixed carbon and the production of H$_2$, but excessive steam will consume heat in the furnace and cause the temperature in the furnace to change. Excessive steam will affect the progress of the reaction.

3.1.4 | Effect of reaction temperature

Under the conditions of S/B = 1.25 and peroxide coefficient 0.2, the effects of different temperatures on the reaction were investigated. The experimental results are shown in Figure 6.

As shown in Figure 6, when the temperature increased from 700°C to 800°C, the volume concentration of H$_2$ in the synthesis gas increased from 37.28% to 43.06%, the volume concentration of CO increased slightly from 16.38% to 16.42%, and the volume concentration of CO$_2$ decreased from 44.36% to 38.40%. When the temperature ranged from 800°C to 900°C, the volume concentration of H$_2$ decreased to 38.09%, the volume concentration of CO increased from 16.42% to 18.57%, and the volume concentration of CO$_2$ increased from 38.40% to 41.67%. The carbon conversion rate continuously increased when the temperature increased: from 700°C to 800°C, the carbon conversion rate increased from 64.02% to 78.22%; when the temperature increased to 900°C, the carbon conversion rate reached a maximum value of 81.44%. The low calorific value of synthesis gas reached the maximum at 800°C. The yield increased greatly from 700°C to 800°C, from 0.94 Nm^3/kg to 1.25 Nm^3/kg, a 32.97% increase. As the temperature continued to rise, the yield began to decline.

Therefore, increasing the temperature appropriately can promote the gasification reaction, increase the carbon conversion rate, and increase the volume concentration of H$_2$ in the synthesis gas. Under these working conditions, the optimal gasification reaction temperature is 800°C.

Properly increasing the temperature can promote the pyrolysis of biomass, promote the lattice oxygen in the oxygen carrier to participate in the reaction, thereby promoting the chemical looping gasification reaction. However, temperature that is too high will cause coking in the CLG process, reducing the synthesis gas hydrogen production and heating value.

3.2 | Fe/Ni/K research

3.2.1 | Effect of loading alkali metal

During the gasification reaction, the presence of alkali metal can improve the activity of oxygen carrier and promote the generation of H$_2$. In this experiment, under the conditions of reaction temperature of 800°C, peroxide coefficient of 0.2, and steam/biomass ratio of 1.25, Fe/Ni bimetallic oxygen carrier was modified by loading an alkali metal to investigate the effects of different mass ratios of alkali metal on the reaction. The experimental results are shown in Figure 7.
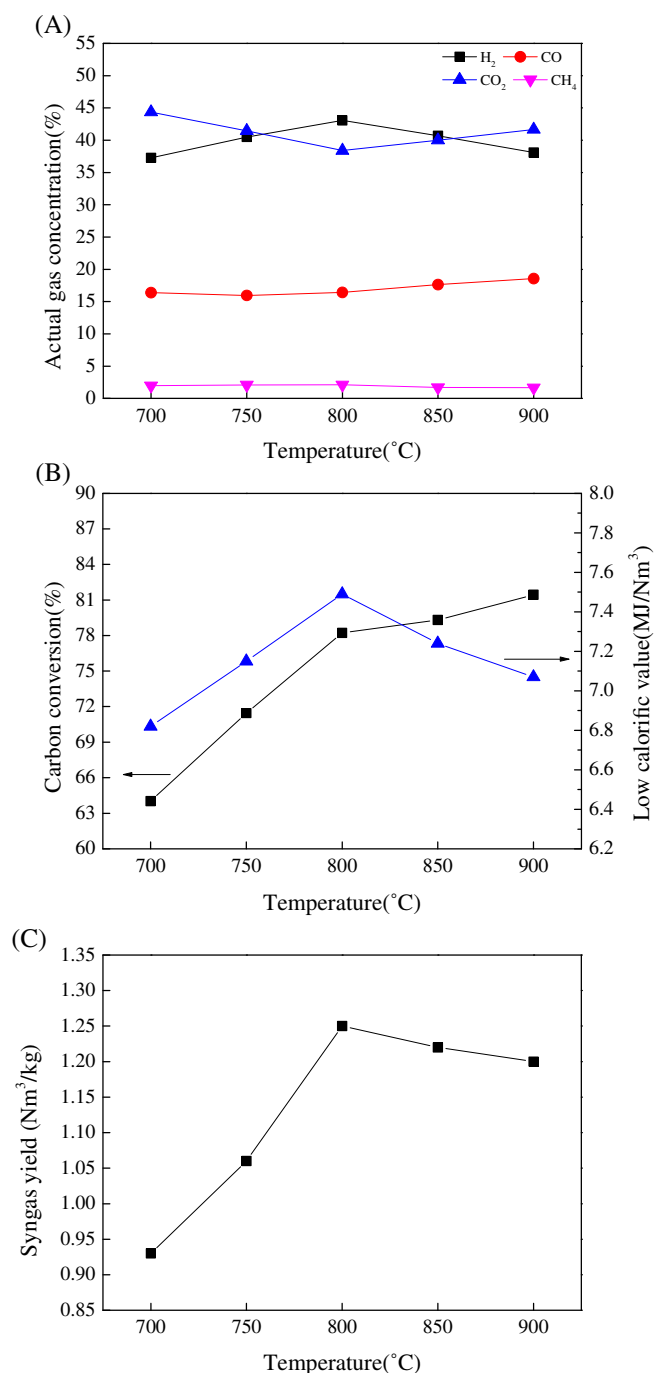
(A)

(B)

(C)

FIGURE 6 Effect of reaction temperature: A, syngas composition; B, carbon conversation rate and low calorific value; C, syngas yield. Reaction conditions: O/B = 0.2, S/B = 1.25, N_2 flow rate of 60 mL/min, reaction time of 50 minutes [Colour figure can be viewed at wileyonlinelibrary.com]

As shown in Figure 7, when the mass ratio of loaded alkali metal, K_2CO_3, was increased from 0% to 5%, the volume concentration of H_2 in synthesis gas increased from 43.06% to 47.83%, the volume concentration of CO increased slightly from 16.42% to 17.62%, and the volume concentration of CO_2 decreased from 38.40% to 32.98%.

While continuing to increase the mass ratio of K_2CO_3, the volume concentration of H_2 in the synthesis gas started to decrease. Therefore, loading an appropriate proportion of alkali metal, K_2CO_3, can promote the generation of H_2 and improve the quality of synthesis gas.

When the mass ratio of the loaded alkali metal, K_2CO_3, was increased from 0% to 5%, the carbon conversion rate increased from 78.22% to 85.44%, the corresponding low calorific value of synthesis gas increased from 7.49 MJ/Nm^3 to 7.97 MJ/Nm^3, and the corresponding yield increased from 1.25 Nm^3/kg to 1.49 Nm^3/kg, a 19.20% increase. When the mass ratio of alkali metal, K_2CO_3, was increased above 5%, although the carbon conversion rate increased slightly at a mass ratio of 7%, the volume concentration of H_2 in the syngas decreased to 45.06%, and the low calorific value also began to decrease. Loading an appropriate proportion of alkali metal K can reduce the activation energy of the gasification reaction; at the same time, alkali metal K can also promote the pyrolysis and reforming of macromolecular organic compounds in biomass, promote the generation of small molecular substances, such as CO and H_2, thereby improving the hydrogen content of syngas.[34]

However, excessive alkali metal will occupy the pores of the oxygen carrier, resulting in the production of more coke, affecting the catalytic efficiency and cyclic reaction performance of the oxygen carrier, thereby reducing the syngas production and calorific value. Under these working conditions, the modification effect is best when the mass ratio of Fe-Ni oxygen carrier is 5% alkali metal.

3.2.2 | Effect of cycles

Under the conditions of reaction temperature of 800°C, O/B = 0.2, and S/B = 1.25, the influence of cycles was investigated. The carrier gas was N_2, the oxidizing gas was O_2, and the flow rate was 60 mL/min. After the reduction reaction was completed for 50 minutes, the N_2 gas path was switched to the O_2 gas path to oxidize the oxygen carrier for 50 minutes. The experimental results are shown in Figure 8.

As shown in Figure 8, with increased cycles, the volume concentration of H_2 in the synthesis gas first decreased and remained basically the same after 10 cycles, then in the 15th cycle was 45.64%; the volume concentration of CO slowly decreased and stabilized after 10 cycles, and in the 15th cycle was 15.49%; and the volume concentration of CO_2 kept rising, and the growth slowed down after 10 cycles, reaching 36.97% in the 15th cycle. As the number of cycles increased, the carbon conversion rate generally showed a slow decline and tended to be stable after 10 cycles. In addition, the low calorific value and yield of synthesis gas decreased apparently at first and
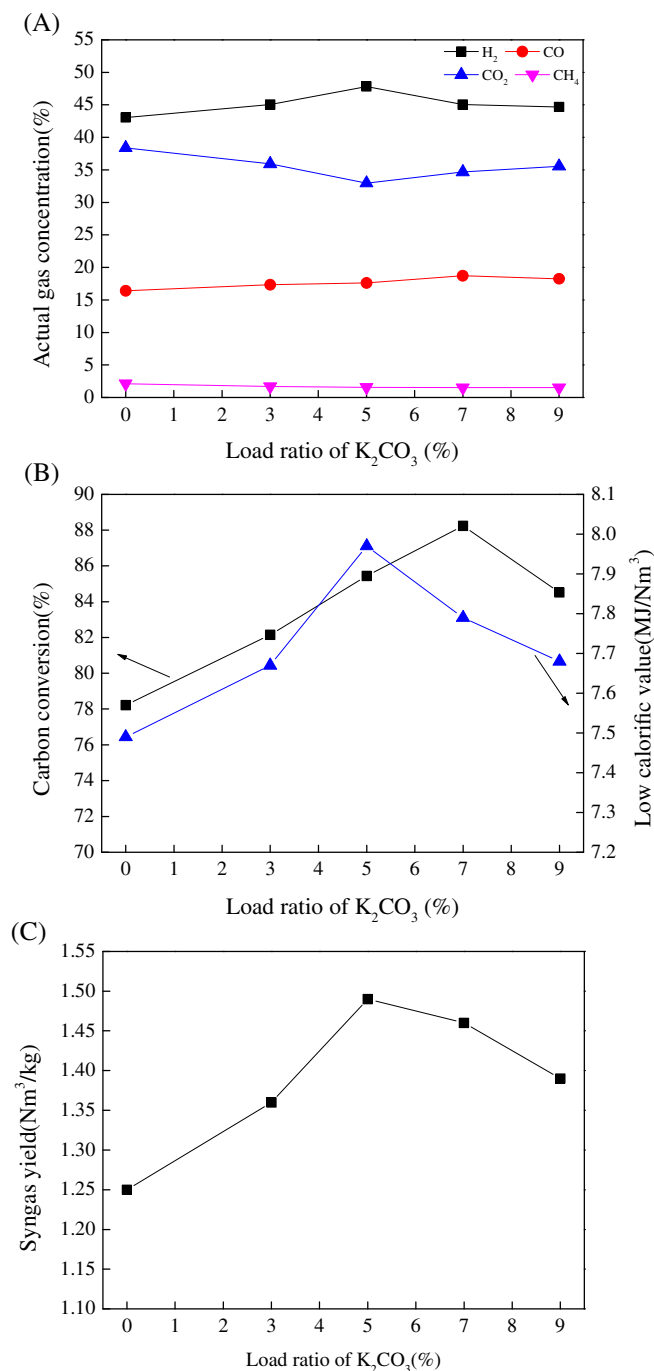
FIGURE 7 Effect of loading alkali metal: A, syngas composition; B, carbon conversion rate and low calorific value; C, syngas yield. Reaction conditions: T = 800°C, O/B = 0.2, S/B = 1.25, N_2 flow rate of 60 mL/min, reaction time of 50 minutes [Colour figure can be viewed at wileyonlinelibrary.com]
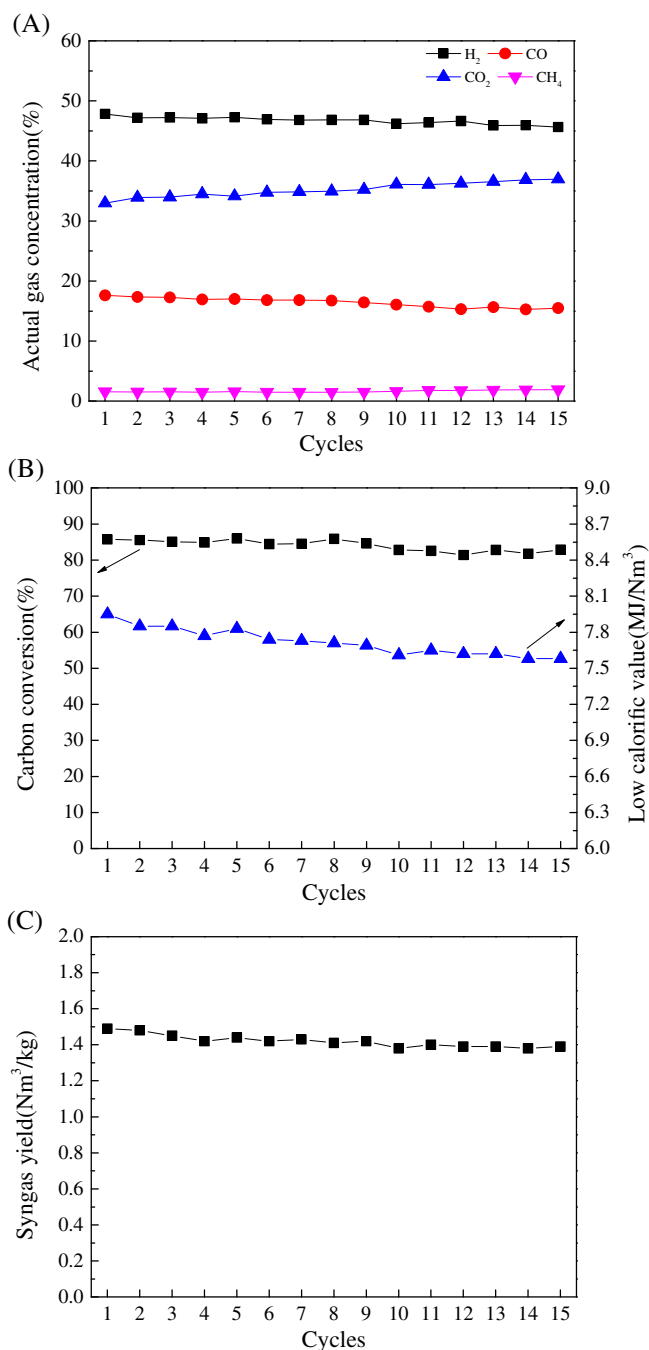
FIGURE 8 Effect of cycles: A, syngas composition; B, carbon conversion rate and low calorific value; C, syngas yield. Reaction conditions: T = 800°C, O/B = 0.2, S/B = 1.25, N_2/O_2 flow rate of 60 mL/min, reaction time of 50 minutes [Colour figure can be viewed at wileyonlinelibrary.com]

stabilized after 10 cycles. After 15 cycles of reaction, the volume concentration of H_2 in the synthesis gas was stable above 45%, the carbon conversion rate was stable above 80%, the low calorific value was stable above 7.5 MJ/Nm^3, and yield was stable above 1.35 Nm^3/kg. Therefore, the activity of the oxygen carrier was well maintained.

3.2.3 | Phase analysis of oxygen carriers

The alkali metal modified iron-nickel composite oxygen carrier was selected to carry out chemical looping gasification cycle experiments for 15 cycles, and the reacted oxygen carrier was characterized by XRD. Figure 9 shows

an XRD characterization diagram of fresh oxygen carrier and oxygen carrier after 15 cycles.

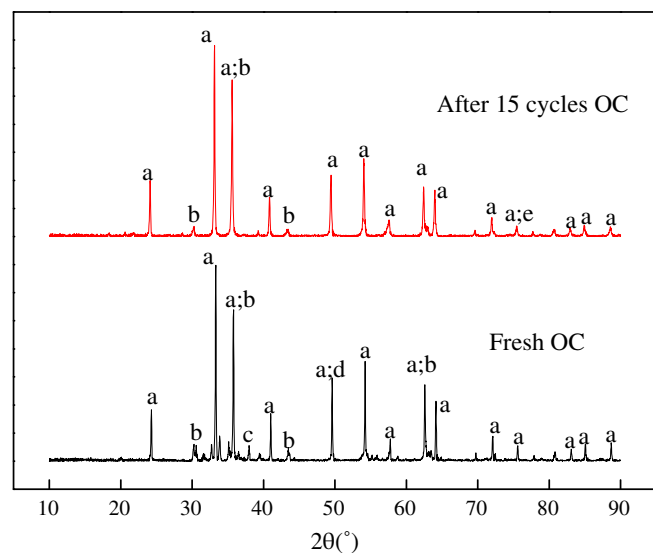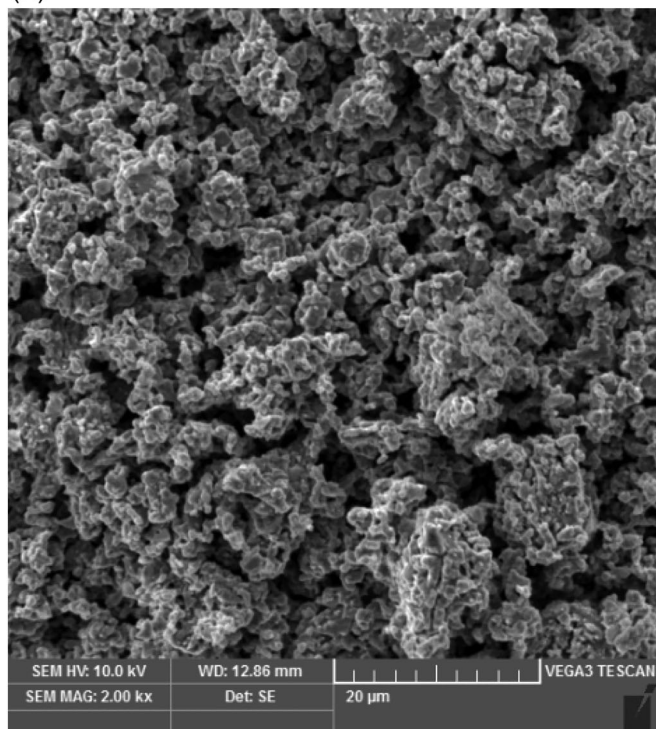As can be seen in Figure 9, XRD characterization results show that the main components of fresh oxygen carrier are Fe_2O_3, $NiFe_2O_4$, and K_2O, and the alkali metal exists in the form of K_2O. In contrast, there is no K_2O peak in the XRD of the oxygen carrier after 15 cycles; a new NiO peak is added, and the Fe (Ni) alloy peak is reduced. This shows that, after multiple cycles, the alkali metal in the oxygen carrier will be lost, and the Fe (Ni) spinel structure will be damaged, which are two important reasons for the decreased activity of the oxygen carrier.

3.2.4 | Micromorphological analysis of oxygen carrier

The oxygen carrier with the best proportion of iron and nickel modified by alkali metal was selected to carry out a chemical looping gasification cycle experiment 15 times, and the reacted oxygen carrier was characterized by SEM. Figure 10 shows an SEM characterization picture of fresh oxygen carrier and oxygen carrier after 15 cycles, in which the magnification is 2000 times.

As shown in Figure 10, clear pores were distributed on the surface of the fresh oxygen carrier, and the pores were disordered. However, the surface of the oxygen carrier after 15 cycles was compact and the structure was uniform. This shows that, with increased cycles, the number and diameter of pores of the oxygen carrier will
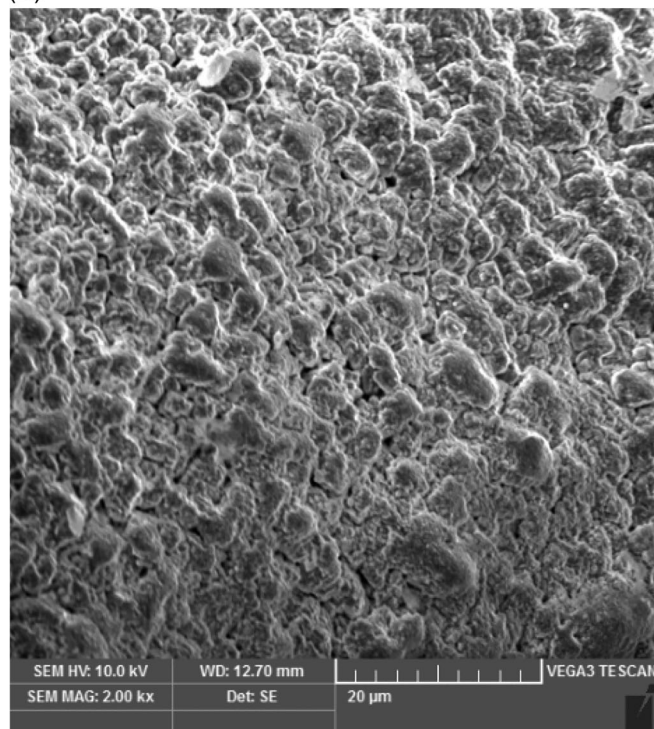

FIGURE 9 XRD characterization of fresh oxygen carrier (OC) and OC after 15 cycles: A, Fe_2O_3; B, $NiFe_2O_4$; C, $Ni_{0.4}Fe_{2.6}O_4$; D, K_2O; E, NiO [Colour figure can be viewed at wileyonlinelibrary.com]

FIGURE 10 SEM characterization of A, fresh OC and B, OC after 15 cycles

TABLE 2 Mesoporous analysis of oxygen carrier

Sample	Surface area (m^2/g)	Pore volume (cm^3/g)	Pore diameter (nm)
Fresh OC	1.827	0.007	3.794
OC after 15 cycles	1.349	0.002	3.373

be significantly reduced during long-term alternating reduction-oxidation reaction, forming a uniform and compact surface, which will inhibit the reaction between the gas and the oxygen carrier, which is also an important reason for deactivation of the oxygen carrier.

3.2.5 | Mesoporous analysis of oxygen carrier

The best ratio of Fe-Ni composite oxygen carrier modified by alkali metal was selected for a chemical looping gasification cycle experiment with 15 cycles, and the oxygen carrier after the reaction was characterized by BET. Table 2 shows the BET characterization results of fresh oxygen carrier and oxygen carrier after 15 cycles.

As shown in Table 2, after 15 cycles with fresh oxygen carrier, the specific surface area decreased from 1.827 m^2/g to 1.349 m^2/g and the pore diameter decreased from 3.794 nm to 3.373 nm. The reduced specific surface area and pore diameter are not conducive to the redox reaction between sawdust particles and oxygen carrier. The pore volume decreased from 0.007 cm^3/g to 0.002 cm^3/g, and it can be seen that the pore volume was greatly reduced. Combined with the electron microscopic characterization shown in Figure 10, it can be seen that there were clear disordered pores on the surface of the fresh oxygen carrier particles, and the surface of the oxygen carrier particles after 15 cycles formed an apparent dense surface. Therefore, the decreased activity can be attributed to the reduced specific surface area, pore size, and pore volume of oxygen carrier particles.

4 | CONCLUSIONS

1. An appropriate amount of NiO loaded on the Fe-based oxygen carrier can increase the activity and promote the progress of the gasification reaction. The best NiO loading was 3 wt%. The volume concentration of H_2 in the synthesis gas is 43.06%, and the total low calorific value reached 9.3625 MJ/kg.
2. For Fe/Ni bimetallic oxygen carrier, modification with an appropriate proportion of alkali metal can promote the gasification reaction and increase the volume concentration of H_2 in synthesis gas. The best alkali metal

loading was 3 wt%. The corresponding volume concentration of H_2 in synthesis gas reached 47.83%, and the total low calorific value reached 11.88 MJ/Nm^3.
3. With increased cycles, the activity of oxygen carriers decreased. The main reason is that, after 15 cycles, the alkali metal is lost, the structure of Fe-Ni spinel of the oxygen carrier is damaged, free NiO phase appeared, and the surface aperture of the oxygen carrier is significantly reduced.

DATA AVAILABILITY STATEMENT
The data that support the findings of this study are available from the corresponding author upon reasonable request.

ORCID
Ge Pu https://orcid.org/0000-0003-3080-4088

REFERENCES
1. Liu F, Wu X, Zhang X, et al. Co-use of organic herbal residue and red mud waste for syngas production by chemical looping gasification. *Int J Energy Res*. 2020;45(5):7666-7680.
2. Pan Y, Tursun Y, Abduhani H, Turap Y, Abulizi A, Talifua D. Chemical looping gasification of cotton stalk with bimetallic cu/Ni/olivine as oxygen carrier. *Int J Energy Res*. 2020;44(9): 7268-7282.
3. Ubando A, Chen W-H, Show P-L, et al. Kinetic and thermodynamic analysis of iron oxide reduction by graphite for CO_2 mitigation in chemical-looping combustion. *Int J Energy Res*. 2020; 44(5):3865-3882.
4. Xue Z, Du X, Rac V, et al. Partial oxidation of NO by H_2O_2 and afterward reduction by NH_3-selective catalytic reduction: an efficient method for NO removal. *Ind Eng Chem Res*. 2020;59 (20):9393-9397.
5. Liu F, Yang L, Wu X, Zhang X, Liu Y. Bauxite waste with low Fe_2O_3 and high Na concentration as a promising oxygen carrier in chemical looping combustion. *Int J Energy Res*. 2020;44(5): 3790-3800.
6. Zhang X, Yang S, Xie X, et al. Stoichiometric synthesis of Fe/Ca$_x$O catalysts from tailored layered double hydroxide

precursors for syngas production and tar removal in biomass gasification. *J Anal Appl Pyrolysis*. 2016;120(7):371-378.

7. Liu C, Chen D, Wang W. Hydrogen-rich syngas production from chemical looping steam reforming of bio-oil model compound: effect of bimetal on $LaNi_{0.8}M_{0.2}O_3$ (M = Fe, Co, Cu, and Mn). *Int J Energy Res*. 2019;43(9):4534-4545.

8. Wang X, Xu T, Jin X, et al. CuO supported on olivine as an oxygen carrier in chemical looping processes with pine sawdust used as fuel. *Chem Eng J*. 2017;330(11):480-490.

9. Zhu L, Chen H, Fan J, Jiang P. Thermo-economic investigation: an insight tool to analyze NGCC with calcium-looping process and with chemical-looping combustion for CO_2 capture. *Int J Energy Res*. 2016;40(14):1908-1924.

10. Xiao Z, Hui Z, Vineet S, et al. Biomass-based chemical looping technologies: the good, the bad and the future. *Energy Environ Sci*. 2017;10(9):1885-1910.

11. Qin W, Chen S, Ma B, et al. Methanol solution promoting cotton fiber chemical looping gasification for high H_2/CO ratio syngas. *Int J Hydrog Energy*. 2019;44(14):7149-7157.

12. Ahmed H, Ibrahim D. Comparative assessment of various gasification fuels with waste tires for hydrogen production. *Int J Hydrog Energy*. 2019;44(34):18818–18826.

13. Shakirudeen A, Syeda H, Mohammad H, et al. Eggshell as a potential CO_2 sorbent in the calcium looping gasification of biomass. *Waste Manag*. 2018;80:274-284.

14. Demirel Y, Matzen M, Winters C, et al. Capturing and using CO_2 as feedstock with chemical looping and hydrothermal technologies. *Int J Energy Res*. 2015;39(8):1011-1047.

15. Lee J, Lee H, Cho H, et al. Redox reactivity of titania-doped YSZ-promoted iron-based oxygen carrier over multiple redox cycles for chemical looping reforming of methane and hydrogen production. *Int J Energy Res*. 2020;44(6):4919-4932.

16. Kale GR, Kulkarni B, Bharadwaj K. Chemical looping reforming of ethanol for syngas generation: a theoretical investigation. *Int J Energy Res*. 2013;37(6):645-656.

17. Moghtaderi B. Application of chemical looping concept for air separation at high temperatures. *Energy Fuel*. 2013;24(1):190-198.

18. Wei G, He F, Zhao Z, et al. Performance of Fe–Ni bimetallic oxygen carriers for chemical looping gasification of biomass in a $10kW_{th}$, interconnected circulating fluidized bed reactor. *Int J Hydrog Energy*. 2015;40(46):16021–16032.

19. Xu D, Zhang Y, Hsieh TL, et al. A novel chemical looping partial oxidation process for thermochemical conversion of biomass to syngas. *Appl Energy*. 2018;222:119-131.

20. Pérez-Vega R, Abad A, Gayán P, de Diego LF, García-Labiano F, Adánez J. Development of $(Mn_{0.77}Fe_{0.23})_2O_3$, particles as an oxygen carrier for coal combustion with CO_2, capture via in-situ gasification chemical looping combustion(iG-CLC) aided by oxygen uncoupling (CLOU). *Fuel Process Technol*. 2017;164:69-79.

21. Jeremias M, Pohorely M, Svoboda K, et al. Gasification of biomass with CO_2 and H_2O mixtures in a catalytic fluidised bed. *Fuel*. 2017;210:605-610.

22. Huang Z, He F, Feng YP, et al. Synthesis gas production through biomass direct chemical looping conversion with natural hematite as an oxygen carrier. *Bioresour Technol*. 2013;140:138-145.

23. Chen L, Yang L, Liu F, Nikolic HS, Fan Z, Liu K. Evaluation of multi-functional iron-based carrier from bauxite residual for H_2-rich syngas production via chemical-looping gasification. *Fuel Process Technol*. 2017;156:185-194.

24. Xiao R, Zhang S, Peng S, Shen D, Liu K. Use of heavy fraction of bio-oil as fuel for hydrogen production in iron-based chemical looping process. *Int J Hydrog Energy*. 2014;39:19955–19969.

25. Zheng M, Zhong S, Li K, et al. Characteristics of CaS–CaO oxidation for chemical looping combustion with a $CaSO_4$-based oxygen carrier. *Energy Fuel*. 2017;31(12):13842–13851.

26. Kuo PC, Chen JR, Wu W, Chang JS. Hydrogen production from biomass using iron-based chemical looping technology: validation, optimization, and efficiency. *Chem Eng J*. 2018;337(1):405-415.

27. Xue N, Wang Z, Wu J, et al. Effect of equivalence ratio on the CO selectivity of Fe/Ca-based oxygen carriers in biomass char chemical looping gasification. *Fuel*. 2019;252:220-227.

28. Cho W, Kim C, Jeong S, et al. Activation and reactivity of iron oxides as oxygen carriers for hydrogen production by chemical looping. *Ind Eng Chem Res*. 2015;54:3091-3100.

29. Huang Z, He F, Zhao K, et al. Natural iron ore as an oxygen carrier for biomass chemical looping gasification in a fluidized bed reactor. *J Therm Anal Calorim*. 2014;116:1315-1324.

30. Huang Z, Deng Z, He F, et al. Reactivity investigation on chemical looping gasification of biomass char using nickel ferrite oxygen carrier. *Int J Hydrog Energy*. 2017;42(21):14458–14470.

31. Chen J, Zhao K, Zhao Z, He F, Huang Z, Wei G. Identifying the roles of MFe_2O_4(M=Cu, Ba, Ni, and Co) in the chemical looping reforming of char, pyrolysis gas and tar resulting from biomass pyrolysis. *Int J Hydrog Energy*. 2019;44(10):4674-4687.

32. Feng Y, Wang N, Guo X, Zhang S. Dopant screening of modified Fe_2O_3 oxygen carriers in chemical looping hydrogen production. *Fuel*. 2020;262(2):1-9.

33. Liu S, He F, Huang Z, et al. Screening of $NiFe_2O_4$ nanoparticles as oxygen carrier in chemical looping hydrogen production. *Energy Fuel*. 2016;30(5):4251-4262.

34. Wang L, Shen L, Jiang S, et al. Chemical looping pyrolysis-gasification of biomass for high H_2/CO syngas production. *Int J Energy Res*. 2019;43(1):167-180.